



# Sensitivity of simulations of Plio–Pleistocene climate with the CLIMBER-2 Earth System Model to details of the global carbon cycle

Judit Carrillo<sup>a,b,1</sup> , Michael E. Mann<sup>a,1</sup> , Irina Marinov<sup>a</sup>, Shannon A. Christiansen<sup>a</sup>, Matteo Willeit<sup>c</sup> , and Andrey Ganopolski<sup>f</sup>

Affiliations are included on p. 7.

Contributed by Michael E. Mann; received December 31, 2024; accepted April 26, 2025; reviewed by Hugues Goosse and Mikhail Verbitsky

The Earth system model CLIMBER-2 has been used in past work to successfully reproduce the glacial/interglacial cycles of the Plio–Pleistocene and the Mid-Pleistocene Transition (MPT) from predominantly 40 to 100 ky timescale oscillatory behavior as a function of declining volcanic outgassing and regolith removal. In this study, we further examine the sensitivity of this previous work to varying prescribed levels of volcanic outgassing and regolith extent and the long-term dynamics of the global carbon cycle, affecting the exchange and partitioning of carbon between different Earth system reservoirs and therefore global atmospheric CO<sub>2</sub> concentrations. As volcanic outgassing decreases, CO<sub>2</sub> and land carbon storage decrease, while ocean carbon storage, including CaCO<sub>3</sub> sediment, increases. At volcanic outgassing levels below a threshold value of roughly 5.7 Tmol C yr<sup>-1</sup>, sea level decreases due to land ice formation, leading to increased carbon accumulation in the ocean and decreased carbon in the CaCO<sub>3</sub> sediment reservoir. Our previous finding of strong hysteresis and path dependence in the glacial/interglacial alternation history [J. Carrillo *et al.*, *Proc. Natl. Acad. Sci.* 121, e2322926121 (2024)] appears to be a tenuous climate feature, dependent on the precise representation of carbon cycle processes and, specifically, the numerical precision used in the calculation of certain key state variables in the model's carbon cycle.

climate models | atmospheric carbon dioxide | glacial–interglacial cycles | volcanic outgassing | carbon cycle

Milutin Milankovitch (1–3) theorized that the Quaternary glacial/interglacial cycles were paced by the cyclical changes in boreal summer insolation on timescales of tens to hundreds of kiloyears. Paleoclimate records and model simulations have provided strong support for this theory on the whole. However, it cannot explain the dominant low-frequency, high-amplitude, ~100-ky eccentricity-driven glacial variability that emerges during the Middle Pleistocene Transition (MPT) (between 1.25 to 0.75 My B.P.) or the increase in amplitude and asymmetry of the glacial cycles thereafter (4–8).

Internal mechanisms involving threshold-dependent behavior (3, 7) have been proposed to explain these phenomena. Paillard (6) suggests that existence of three steady Earth system states: “interglacial,” “mild glacial,” and “full glacial” within the framework of astronomical theory. Other possible explanations involve obliquity-period-doubling bifurcation as the result of increased amplitude feedbacks during the MPT (9) and nonlinear responses to eccentricity forcing (5). Raymo *et al.* (10), Huybers and Tziperman (10), and Abe-Ouchi *et al.* (4) among others, suggested a relationship between the MPT and the ice sheet extent. Bintanja and van de Wal (11) argue that the more prominent North American ice sheets of the Late Pleistocene possessed a greater capacity to endure insolation maxima, thereby melting only once every few orbital cycles. Other hypotheses involve changes in ocean carbon chemistry with changing aridity (12), oceanic and atmospheric poleward heat flux (7, 13), ocean stratification impacting ocean–atmosphere CO<sub>2</sub> exchange (14), carbon cycle dynamics (15–17), and Atlantic meridional circulation changes (18).

A compelling mechanistic explanation was more recently offered by Willeit *et al.* (henceforth “W19”) (19) related to the gradual removal of regolith (19, 20), which leads to reduced basal sliding, increasingly large ice sheets, and a transition at the observed timing of the MPT to a strong ~100 ky cycle. More recently, Carrillo *et al.* (21), using the same (CLIMBER-2) model as W19, find evidence of path dependence in this behavior, with the disappearance of the MPT in backward-in-time (“BIT”) integrations of the model. A trend toward depleted regolith and lowered atmospheric CO<sub>2</sub> levels, as observed in forward-in-time (“FIT”) integrations, were both required to reproduce the MPT.

## Significance

Using the CLIMBER-2 model to simulate the Plio–Pleistocene climate evolution, we find that for low (high) volcanic outgassing levels, the carbon system reorganizes itself such that atmospheric CO<sub>2</sub> is lower (higher), land carbon storage is low (high), and ocean carbon storage, including CaCO<sub>3</sub> sediments, is high (low). Low volcanic outgassing and depleted regolith are required to reproduce the Mid-Pleistocene Transition (MPT) toward 100 ky CO<sub>2</sub> cycles. The path dependence in Plio–Pleistocene climate evolution identified in our previous simulations with the CLIMBER-2 model [J. Carrillo *et al.*, *Proc. Natl. Acad. Sci.* 121, e2322926121 (2024)] is greatly reduced in the current simulations, wherein greater numerical precision is used in the calculation of certain state variables in the model's carbon cycle.

Author contributions: J.C. and M.E.M. designed research; J.C., I.M., and M.W. performed research; J.C. analyzed data; and J.C., M.E.M., I.M., S.A.C., M.W., and A.G. wrote the paper.

Reviewers: H.G., University of Louvain-la-neuve; and M.V., Gen5 Group, LLC.

The authors declare no competing interest.

Copyright © 2025 the Author(s). Published by PNAS. This article is distributed under Creative Commons Attribution-NonCommercial-NoDerivatives License 4.0 (CC BY-NC-ND).

<sup>1</sup>To whom correspondence may be addressed. Email: juditcp@sas.upenn.edu or mmann00@sas.upenn.edu.

This article contains supporting information online at <https://www.pnas.org/lookup/suppl/doi:10.1073/pnas.2427236122/-/DCSupplemental>.

Published June 2, 2025.

The role of the carbon cycle— particularly with respect to glacial terminations (5, 22)—deserves particular attention in understanding these findings. The oceanic carbon reservoir has a dominant influence on atmospheric CO<sub>2</sub> levels. The marine biological pump plays a particularly important role, by fixing CO<sub>2</sub> in the upper ocean via primary producers, ultimately transporting that carbon to the deep ocean. Carbon is accumulated in deep waters until it is eventually ventilated at the sea surface. However, some of the fixed carbon is not mineralized but is instead stored for millennia as dissolved organic matter (23). Shackleton et al. (24), show that an MPT-like change in glacial/interglacial cyclicity can be generated using a carbon cycle model in which feedbacks between calcifer populations and ocean alkalinity mediate atmospheric CO<sub>2</sub>. Other features of the oceanic carbon cycle are important. The solid Earth itself plays an important role in carbon cycle behavior relevant to glaciation. During deglaciation, the ablation of glaciers and ice caps reduces ice volume, decompressing the mantle, which increases volcano-generated magma production by depressurization, raising atmospheric CO<sub>2</sub>, causing more warming and deglaciation.

While the level of volcanic outgassing is a critical factor governing long-term Plio–Pleistocene climate evolution, its precise magnitude is uncertain even in the present day (25). In the CLIMBER-2 model, the present-day volcanic outgassing rate was determined from the condition that it balances the average silicate weathering rate on long time scales (26, 27), while W19 introduced a long-term trend in the volcanic outgassing, selecting the level of volcanic outgassing in simulations with the CLIMBER-2 model that best reproduced the Plio–Pleistocene benthic δ<sup>18</sup>O history, thus solving an inverse problem. The same trends in CO<sub>2</sub>, however, could alternatively be achieved by specifying a modest increase in the weathering rate and/or the organic carbon burial in deep-sea sediments (19, 28).

Simulations with coupled climate-ice sheet models (4, 15, 17, 29) can simulate 100 ky glacial cycles even with a constant low (e.g., 220 ppm) CO<sub>2</sub> concentration (4). Atmospheric CO<sub>2</sub> changes, however, strongly amplify the direct response of ice sheets to the orbital forcing (30). Northern Hemisphere ice sheet dynamics are also strongly influenced by regolith removal from glacial erosion processes (5, 19, 20, 31–33). Ice sheets can slide more readily over sediment than bedrock. Moreover, the removed glaciogenic dust, deposited over the southern margins of Northern Hemisphere ice sheets, substantially lowers snow albedo, facilitating melting and hindering the growth of large ice sheets (34–36).

Here, we examine the carbon cycle behavior in the CLIMBER-2 model more closely in an attempt to better understand the role of both regolith removal, volcanic outgassing-driven changes in CO<sub>2</sub>, and their internal interaction with components of the global carbon cycle. In the process of these investigations, we reexamine the findings of strong hysteresis and path dependence in ref. 21 and the dependence of these phenomena on the precision with which key components of the global carbon cycle are represented in the model.

## Results

**Role of different Earth system components in CO<sub>2</sub> variations over the past 3 My.** We assessed the role of different mechanisms on atmospheric CO<sub>2</sub>, volcanic outgassing (denoted as V), removal of regolith, interactive ice sheets, and insolation, in a series of forward-in-time (FIT) experiments starting from the same initial pCO<sub>2</sub> condition (Fig. 1—see *Materials and Methods* and *SI Appendix, Fig. S1* for further details, including descriptions of the prescribed forcings in these experiments).

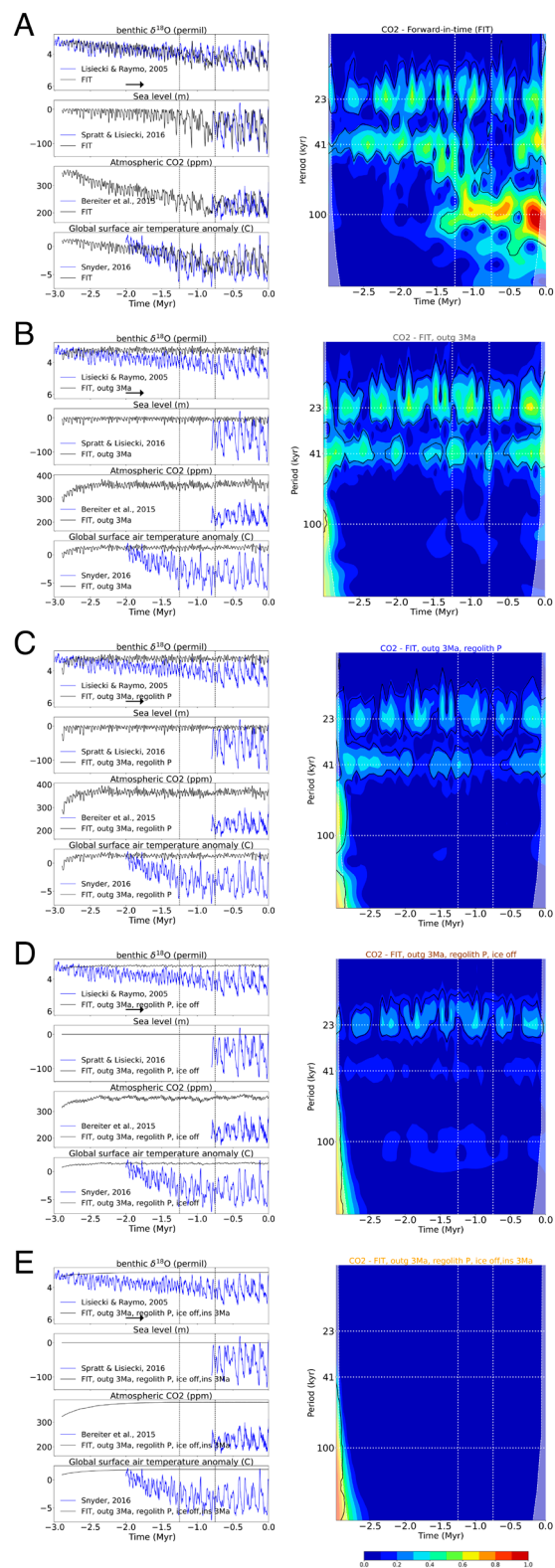


**Fig. 1.** Standard (continuous) simulations from  $-3$  My to present. (A) The reference forward in time (FIT) experiment. (B) FIT with constant volcanic outgassing at levels representative of 3 Ma. (C) FIT with constant volcanic outgassing of 3 Ma and regolith depleted as in the present. (D) Same as C but with the interactive ice sheet module disabled. (E) Same as D but with constant solar insolation as at 3 Ma. (Left) Modeled benthic  $\delta^{18}\text{O}$ , relative sea level, atmospheric CO<sub>2</sub>, and global surface air temperature (all relative to modern preindustrial) (black) compared to the proxy estimates of these quantities [respectively from Lisiecki and Raymo (37), Spratt and Lisiecki (38), Bereiter et al. (39), and Snyder (40)] (blue). The dashed vertical lines mark the MPT. (Right) Wavelet (41) spectra of carbon dioxide. The color scale (Bottom of plot) indicates the normalized amplitude evaluated in 1,000-y steps. The horizontal white lines represent the orbital periods of precession ( $\sim 23$  ky), obliquity ( $\sim 41$  ky), and eccentricity ( $\sim 100$  ky). The dashed vertical lines mark the MPT.

The reference experiment “A” (Fig. 1A) is driven with all prescribed time-dependent forcings. In this experiment, we specified a volcanic outgassing history ( $V$ ), which decreases from 6.2 to 5.3 Tmol C yr<sup>-1</sup> over the course of the 3-My timeframe of the experiment, and a regolith history that best reproduces the proxy data (Fig. 1A). In the remaining experiments, we alternatively disabled different subsystems of the model. In experiment B (Fig. 1B) we maintained constant values for volcanic outgassing  $V$ , setting  $V = 6.2$  Tmol C yr<sup>-1</sup> (corresponding to the conditions at -3 My in experiment A), with regolith as in experiment A. In experiment C (Fig. 1C), volcanic outgassing remained constant as in B, and regolith remained depleted throughout the simulation. In experiment D (Fig. 1D), we kept both volcanic outgassing  $V$  and regolith constant and the ice-sheet module was set as non-interactive. Finally, in experiment E (Fig. 1E), the model was configured as in experiment D, but astronomical forcing was kept constant, with the insolation value corresponding to -3 My.

High values of volcanic outgassing  $V$  in each of the simulations B–E lead to persistent high CO<sub>2</sub> levels, global surface temperature, and sea level, failing to reproduce the broad trends in the paleodata captured in the reference simulation (experiment A). It is instructive to examine the frequency-domain behavior of the simulations. We see from the wavelet spectra of the CO<sub>2</sub> series for each of the experiments (Fig. 1, *Right* column) that none of experiments B–E (Fig. 1) reproduce the MPT or the 100 ky cyclicity seen in the reference simulation. This observation is consistent with Carrillo et al. (21), who underscored the critical importance of the prescribed reduction in volcanic outgassing  $V$ , and corresponding long-term decline in CO<sub>2</sub>, in reproducing these features. A decline in volcanic outgassing and the removal of regolith are both required to reproduce the main features of the glacial/interglacial cycles and the cyclicity transition from 41 to 100 ky during the MPT (19, 21).

The ocean and terrestrial carbon cycle play an important role in the model behavior in these experiments, so it is worth taking a closer look at the role of different components of the climate model. Comparing the experiments with and without interactive ice sheets (Fig. 1 C and D) we see very little difference between long-term mean atmospheric CO<sub>2</sub> levels (*SI Appendix*, Fig. S2, compare red and blue lines). Turning the ice sheets on decreases the Earth carbon storage and increases the ocean carbon storage, with a very close compensation between these changes (*SI Appendix*, Fig. S2, column 1). Total CaCO<sub>3</sub> sedimentation in equilibrium is limited by the weathering flux, such that less burial on shelves leads to more burial in the deep sea (42). However, ice sheet presence reduces the land pool’s carbon content by ~30 PgC. Applying a conversion factor of 0.47 ppm PgC<sup>-1</sup> (43), the difference in carbon stored on land explains the 15 ppm atmospheric CO<sub>2</sub> difference between the experiments with and without interactive ice. The detailed role of ice-sheet dynamics will be discussed in a forthcoming study.

**Role of Volcanic Outgassing.** The imbalance between volcanic outgassing and silicate weathering drives atmospheric CO<sub>2</sub> changes over longer timescales. We performed a series of experiments varying the prescribed volcanic outgassing level  $V$  between 5.2 and 6.3 Tmol C yr<sup>-1</sup>, slightly expanding the range explored over the last 3 My in the simulations by Carrillo et al. (21) of 5.3 to 6.2 Tmol C yr<sup>-1</sup> (*SI Appendix*, Fig. S3 shows the time histories of atmospheric CO<sub>2</sub> and ocean, land, and Earth carbon storage components and CO<sub>2</sub> wavelet spectra for each of these experiments).

In Fig. 2, we summarize the overall (steady-state) carbon balance from these experiments, which are performed with both high regolith (values from 3 My ago, *Left* column) and depleted regolith

(values from present, *Right* column). We find that volcanic outgassing is the first-order driver of CO<sub>2</sub>. Decreasing volcanic outgassing reduces atmospheric CO<sub>2</sub> for both low and high regolith coverage. Atmospheric CO<sub>2</sub> decreases from ~381 ppm when  $V = 6.3$  Tmol C yr<sup>-1</sup> and regolith is high (385 ppm for depleted regolith) to ~219 ppm when  $V = 5.3$  Tmol C yr<sup>-1</sup> and regolith is high (233 ppm for depleted regolith). As volcanic outgassing decreases, atmospheric CO<sub>2</sub>, temperature, and precipitation all decrease (*SI Appendix*, Fig. S4), resulting in a drop in land carbon storage (Fig. 2).

Ocean and Earth carbon storage behave fundamentally differently—and in opposite directions—above and below a threshold of  $V \sim 5.7$  Tmol C yr<sup>-1</sup> (Fig. 2). Low values of  $V$  result in low CO<sub>2</sub> and temperatures below critical levels, favoring the rapid growth of continental ice sheets and larger glacial–interglacial fluctuations. As  $V$  decreases further from 5.7 Tmol C yr<sup>-1</sup>, we find larger fluctuations in surface air temperature, precipitation, sea level, and ice volume (*SI Appendix*, Fig. S4 going from panels C to E and from panels H to J) and in all carbon components of the system (*SI Appendix*, Fig. S3 going from panels C to E, and from panels H to J). These translate into a wider spread around the median for atmospheric CO<sub>2</sub>, ocean, and Earth carbon storage components as  $V$  decreases in Fig. 2). The relative amplitude of the ~100 ky cycle also increases as  $V$  decreases (see wavelet analysis in *SI Appendix*, Fig. S3), consistent with the finding by Carrillo et al. (21) that lowered atmospheric CO<sub>2</sub> levels supporting large continental ice sheets are required for initiation of ~100 ky sawtooth glacial/interglacial oscillations.

It is well known that ocean carbon storage is the major mechanism explaining glacial–interglacial variations. Ocean carbon storage increases during glaciations compared to interglacials, as a result of increases in both the solubility and biological carbon pumps, driven by changes in temperature (e.g., colder waters hold more CO<sub>2</sub>), changes in alkalinity, greater stratification and circulation changes in the Southern Ocean and North Atlantic, and increased iron fertilization and sea ice coverage (e.g., more sea ice coverage in upwelling regions locks more carbon in the ocean). By analyzing Fig. 2 and *SI Appendix*, Fig. S3, we see that as  $V$  decreases from 5.7 Tmol C/y the system attains deeper glacial states (increasing the maximum ocean carbon storage) and spends more and more time in glacial states (which increases the median ocean carbon storage).

During glacial intervals, peaks in ocean carbon storage are partly compensated by drops/lows in Earth carbon storage. To understand this, we need to consider all the major components in the Earth carbon inventory. Reduced chemical (silicate) weathering leads to slower atmospheric CO<sub>2</sub> drawdown.

During glacial periods, more ocean carbon storage leads to more acidic deep waters, reducing CaCO<sub>3</sub> concentrations and resulting in a shallowing of the CaCO<sub>3</sub> lysocline. Additionally, lower surface temperatures and reduced nutrients due to enhanced stratification may reduce the productivity of calcifying plankton. All the above factors act to decrease the burial and preservation of CaCO<sub>3</sub> in deep ocean sediments during glaciations, while sea level decrease reduces the preservation of CaCO<sub>3</sub> at ocean margins.

For volcanic outgassing values  $V = 5.7$  and lower, we can apply equivalent arguments for the responses of the carbon cycle to decreasing  $V$  and resulting cooling of the climate. On the longer (equilibrium) time scales, we see a compensation between the ocean carbon reservoir and the Earth carbon reservoir as volcanic outgassing decreases. At depleted (present-day) regolith levels, a drop in  $V$  (from  $V = 5.7$ ) results in a drop in the Earth carbon reservoir, partly compensating the ocean carbon increase (Fig. 2, median values in the *Right* column).

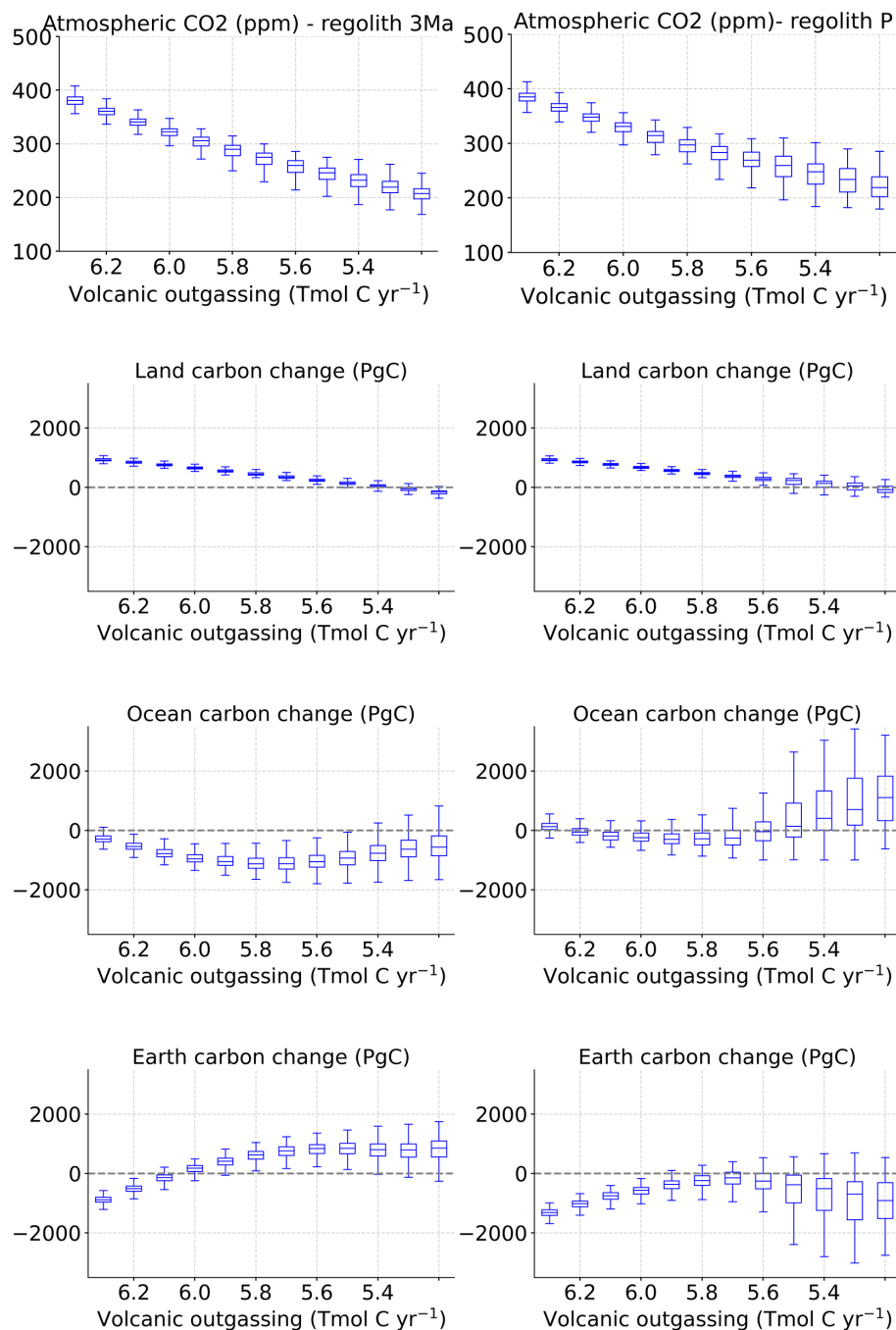


**Fig. 2.** Carbon cycle reservoirs per volcanic outgassing prescribed illustrated with boxplots (center line: median. Box limits: *Upper*—Q3—and *Lower*—Q1—quartiles. The outer range, whiskers, extends from the edges of the box to show the range resulting from glacial/interglacial oscillations). All experiments started with the same initial concentration of CO<sub>2</sub> = 270 ppm. Data corresponding to the first 500 ky were excluded from the boxplots as time to reach equilibrium. (*Left*) Experiments with undepleted (3 Ma) regolith. (*Right*) Experiments with the present-day (depleted) regolith mask.

At higher levels of volcanic outgassing ( $V > 5.7$ ) the behavior of the ocean carbon and Earth carbon storage reverses from the previous case ( $V < 5.7$ ). As  $V$  decreases, ocean carbon now decreases while Earth carbon storage increases. This behavior appears to arise from the competing influence of two opposing factors, including 1) ice-sheet growth, which reduces the shelf area and shifts the calcium carbonate burial from the shelf to the deep ocean, and 2) changes in terrestrial weathering. Further work is underway to better elucidate the competing role of these mechanisms.

The impact of regolith involves both the ocean and Earth carbon components discussed above. More regolith results in greater dust deposition over the ice sheets, thus affecting albedo and surface

mass balance. We find that the Earth carbon storage is larger in the high regolith case (i.e., regolith corresponding to 3 Ma conditions), acting to lower atm CO<sub>2</sub> values compared to the low regolith case (compare *Top* two panels in Fig. 2). The difference in atmospheric CO<sub>2</sub> levels between experiments with depleted and undepleted regolith reaches 14 ppm for  $V$  below 5.5 Tmol C yr<sup>-1</sup> (approximate present-day values). Additionally, the variability in atmospheric CO<sub>2</sub> increases substantially in simulations with depleted regolith, and low levels of volcanic outgassing (Fig. 2), consistent with the greater amplitude glacial/interglacial cycles post-MPT. Throughout these experiments (*SI Appendix, Figs. S3–S5*), we find that eccentricity-timescale ~100 ky spectral peaks are

significant only when regolith is depleted (as it is at Present), and volcanic outgassing is below roughly  $5.7 \text{ Tmol C yr}^{-1}$ .

### Sensitivity to Representation of Carbon Cycle Processes.

Atmospheric  $\text{CO}_2$  results from large amounts of carbon exchanged between reservoirs. The path dependence in  $\text{CO}_2$  evolution (forward vs. back-in-time execution) observed in the previous study by Carrillo et al. (21) is highly dependent on carbon cycle dynamics as explored in the previous section, which are seen to exhibit threshold-dependent sensitivity to changing volcanic outgassing parameter  $V$ . In attempting to understand this sensitivity better, we more closely examined the details of the CLIMBER-2 carbon cycle submodel. These investigations led to an updating of the model to increase the numerical precision (from single to double precision) of several key state variables in the carbon cycle submodel, including specifically the airborne flux of volcanically outgassed  $\text{CO}_2$ , the consumption of  $\text{CO}_2$  due to terrestrial weathering of carbonate and the silicate flux (*Materials and Methods*).

While a change from single to double precision in a few variables might seem like a small modification, these are key state variables in the carbon cycle model, and relatively small differences in annual fluxes have a magnified impact over the millions-of-year time integrations in our simulations, particularly given the existence of threshold-dependent carbon cycle behavior as characterized in the previous section. In Fig. 3, we compare the FIT and BIT experiments using both the previous and updated version of the model. The same forcings (i.e., insolation, regolith removal, and volcanic outgassing) were prescribed in these experiments. The only difference from the previous study is the precision of the variables associated with the carbon cycle fluxes.

The initial state in these experiments has an impact on the precise evolution of the model (*SI Appendix, Fig. S6*), but volcanic outgassing plays the key role in determining the evolution of  $\text{CO}_2$ . Regardless of initial state, the model fails to reproduce the glacial period between  $-500$  and  $-400$  ky which occurred during an interval of very weak orbital forcing. It has previously been suggested that current climate–ice sheet models fail to fully capture nonlinear mechanisms that might be important in explaining this particular interval (15, 19).

Nonetheless, the model is capable of reproducing important nonlinearities in the system. *SI Appendix, Fig. S7* summarizes experiments in which the  $V$  forcing of the standard FIT experiment (which varies from  $6.2 \text{ Tmol C yr}^{-1}$  during the Late Pliocene

to  $5.3 \text{ Tmol C yr}^{-1}$  in the Present), has been adjusted by the following fixed amounts over the duration of the experiments: A)  $+0.5$ , B)  $+0.3$ , C)  $+0.1$ , D)  $-0.1$ , E)  $-0.1$ , F)  $-0.3$ , and G)  $-0.5 \text{ Tmol C yr}^{-1}$ . These experiments demonstrate a high sensitivity in the carbon cycle to small changes in the  $V$  forcing. In experiment A (addition of  $+0.5 \text{ Tmol C yr}^{-1}$ )  $V$  remains at or above  $5.7 \text{ Tmol C yr}^{-1}$ , and carbon accumulates in the Earth reservoir. By contrast, in experiment G (subtraction of  $0.5 \text{ Tmol C yr}^{-1}$ ),  $V$  remains at or below  $5.7 \text{ Tmol C yr}^{-1}$  over the entire simulation, leading to an accumulation of carbon in the ocean.

The discrepancy observed between experiments E and F is particularly remarkable; with only a small addition of  $0.2 \text{ Tmol C yr}^{-1}$  (roughly 20% of the change in  $V$  during the three million-year period analyzed), a tipping point is identified at which carbon is sequestered in the ocean, resulting in a sudden decrease in atmospheric  $\text{CO}_2$  concentration.

These experiments thus illustrate the dramatic nonlinearity of the carbon cycle behavior in this model, which expresses itself as a substantial sensitivity to relatively small changes in forcing. This finding helps explicate our finding that the precise evolution of climate during the Plio–Pleistocene era is sensitive to the numerical precision of carbon cycle calculations within the model since small differences in carbon fluxes result in substantial differences in carbon reservoir amounts over long periods. It also, however, hints at the possibility that the Plio–Pleistocene climate system is capable of exhibiting intransitive and chaotic behavior, as discussed later.

Unlike the previous model, the updated FIT and BIT experiments now exhibit very similar long-term trends including the timing and character of the MPT. This long-term (My) trend in  $\text{CO}_2$  and the MPT are driven by the combined long-term trends in volcanic outgassing and regolith distribution, with little evidence of any path dependence in the overall long-term trends. In the current FIT and BIT experiments, we see a large increase in ocean carbon storage from about 2 to 0.8 My, partly compensated by the Earth carbon storage, which explains the reduction in atmospheric  $\text{CO}_2$  over this period. The ocean carbon storage increase is larger than in the BIT experiments of Carrillo et al. (21).

Although much of the previously published difference between the FIT and BIT experiments largely disappears when the numerical precision is increased in key carbon cycle state variables, some differences nonetheless remain. The BIT experiments show greater ocean carbon storage than the FIT experiments, amounting to a mean difference in atmospheric  $\text{CO}_2$  of  $\sim 30$  ppm from 3 to

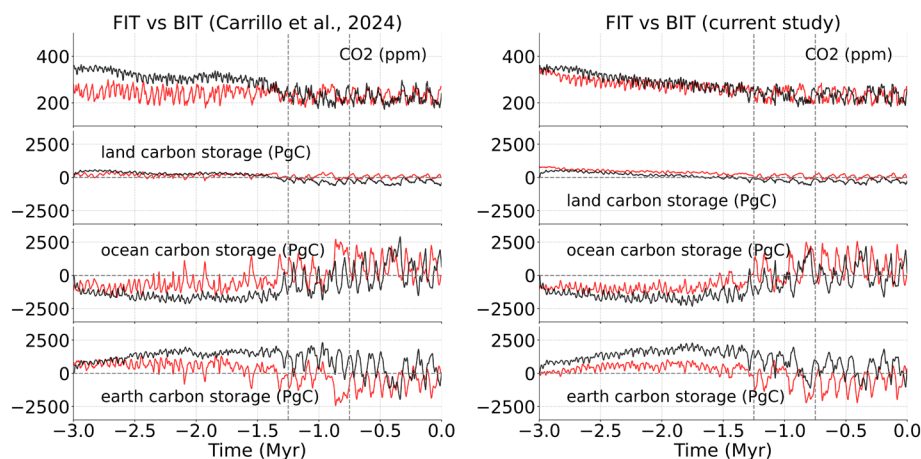


**Fig. 3.** Comparison between forward-in-time (FIT-black) and back-in-time (BIT-red) experiments for original Carrillo et al. (21) version (*Left*) and current (*Right*) version of the carbon cycle model. Shown are atmospheric  $\text{CO}_2$  (ppm), and land, ocean, and total carbon reservoirs (in PgC). The dashed vertical lines mark the Mid-Pleistocene Transition (MPT).

2.5 Ma. Critical sinks or sources of atmospheric CO<sub>2</sub> related to, e.g., the chemical weathering of silicate rocks (44) take hundreds of thousands of years to equilibrate, explaining the difference in the phasing of atmospheric CO<sub>2</sub> in both experiments. Notable differences between the FIT and BIT simulations also remain on shorter timescales, with the BIT experiments failing to capture as well the observed phasing of the 100 ky cycles during the past 1 My, due to the lagged equilibration of the Earth system.

## Discussion

In this study, we further examined details of the Plio–Pleistocene climate evolution in the CLIMBER-2 Earth system model. This model includes coupled oceanic, atmospheric, ice sheets, and biogeochemical processes relevant to long-term climate and Earth system variability, including a comprehensive global carbon cycle model (21, 45), to assess how carbon is partitioned between the reservoirs for differing levels of volcanic outgassing and for different regolith distributions.

Our simulations demonstrate a clear threshold response of the model when volcanic outgassing levels fall below roughly 5.7 Tmol C yr<sup>-1</sup> which relates to fundamental differences in the behavior of key components of the global carbon cycle above and below this level. This nonlinear behavior appears both with undepleted and depleted regolith and amplifies the sensitivity of long-term simulation of the model to small differences in carbon fluxes over long periods of time. Indeed, when we update the model carbon cycle to employ double precision in calculations involving these fluxes (specifically, the airborne flux of volcanically outgassed CO<sub>2</sub>, the consumption of atmospheric CO<sub>2</sub> due to terrestrial weathering of carbonate and the silicate flux), the model displays a more linear response of atmospheric CO<sub>2</sub> concentration to volcanic outgassing  $V$  over the Plio–Pleistocene interval analyzed.

The low-precision arithmetic of the previous version of the carbon cycle model interacts with threshold-dependent processes to yield spurious long-term drifts in the carbon budget. As a result, the path-dependent behavior and hysteresis found in the previous study (21) largely disappear with the more accurate carbon cycle representation. The forward and backward integrations (i.e., FIT and BIT) of the model show similar long-term behavior. In particular, the low CO<sub>2</sub> and cold conditions during the early Pleistocene in the BIT experiment in the previous study largely disappear. Future investigation will focus on a more detailed analysis of the ice sheet mechanisms that impact the carbon cycle. Our current simulations nonetheless confirm one of the key findings of our earlier study, namely that a combination of both the

$$\text{Earth carbon flux} \left( \frac{\text{GtC}}{\text{yr}} \right) = \text{airborne flux of volcanic CO}_2 + \text{Atmospheric consumption of CO}_2 \text{ due to terrestrial weathering of carbonate and silicate flux} \\ + \text{bicarbonate flux from the land to the ocean from continental weathering} + \text{CaCO}_3 \text{ burial on shelf (coral reefs) and in the deep sea} \quad [2]$$

long-term decrease in volcanic outgassing and regolith removal through successive glacial expansion and retraction, is necessary and sufficient to reproduce both the long-term trend toward increased glaciation over the course of the Plio–Pleistocene and the Mid-Pleistocene Transition (i.e., MPT) from low-amplitude obliquity (~41 ky) to large-amplitude eccentricity-dominated, 100 ky glacial/interglacial cycles during the 1.25 to 0.75 My Mid-Pleistocene interval.

Our current study demonstrates, at a minimum, the critical importance of using high numerical precision in Earth system modeling experiments that involve potentially nonlinear dynamical climate behavior, very small annual fluxes, and extremely long timescales. But it might demonstrate something deeper. Saltzman

(46) noted that the Pleistocene glacial/interglacial cycles are controlled by small differences in very large fluxes of mass and energy making them susceptible to both forced and free oscillatory behavior characteristic of a nonlinear, long memory dynamical system. While Saltzman was focused on the tenuous long-term balance between accumulation and ablation of ice, our work shows that a similar situation seems to hold with the global carbon cycle. Such sensitivity to initial carbon cycle conditions has indeed been observed in past dynamical modeling of the Pleistocene glacial/interglacial cycles. For example, the Shackleton et al. (24) study discussed earlier, which used a dynamical ocean calcifier-alkalinity model to simulate global CO<sub>2</sub> behavior on orbital timescales, found that the time evolution of their model was highly sensitive to initial ocean alkalinity levels. Future work should further assess whether the highly sensitive carbon cycle behavior identified in the present study hints at a more fundamental property of the climate system on orbital and longer timescales.

## Materials and Methods

**Model.** CLIMBER-2 is an Earth system model (19, 22, 26, 47–49) of intermediate complexity. It includes a statistical-dynamical atmospheric model, ocean model, dynamical terrestrial vegetation model, ocean carbon cycle model, aeolian dust cycle, and other components. The model incorporates long-term terrestrial carbon pools such as permafrost carbon, peat, and carbon buried beneath the ice sheets, accounting for peat accumulation (25). The ocean carbon cycle includes modules for marine biota, oceanic biogeochemistry, marine sediments, and iron fertilization effects. The thermomechanical ice-sheet model SICOPOLIS (see below for further description) is applied only to the Northern Hemisphere, assuming the Antarctic ice sheet contributes 10% to the global sea level variations.

CLIMBER-2 works with a coarse spatial resolution, allowing only continental-scale features and three oceanic basins to be resolved. However, this parameterization allows a reasonable computational speed in experiments lasting millions of years.

CLIMBER-2, including the global carbon cycle model (26, 47), was previously used to reproduce characteristics of the last four glacial cycles (30) and variation over the past 3 My (19, 21). The model accounts for carbon exchange among geological, land, and ocean carbon reservoirs.

The atmospheric CO<sub>2</sub> concentration is computed by the model from the following equation, using a conversion factor of 0.47 ppm PgC<sup>-1</sup> (43).

$$p\text{CO}_2(t+dt) (\text{ppm}) = p\text{CO}_2(t) - 0.47 * \int_t^{t+dt} (\text{Ocean carbon flux} \\ + \text{Land carbon flux} + \text{Earth carbon flux}) (\text{GtC/yr}) dt, \quad [1]$$

where

Note that the airborne flux of volcanic CO<sub>2</sub> is a calculated variable, differing from the (specified) volcanic outgassing  $V$  in the presence of continental ice sheets which exhibit their own specific interactions with atmospheric carbon.

Following Huybers and Langmuir (45), Ganopolski and Brovkin (30) introduced a dependence in the CLIMBER-2 model of the airborne flux of volcanic CO<sub>2</sub> (defined as “ $O$ ”) on the rate of sea level change. They prescribed volcanic outgassing as depending linearly on the time derivative of sea level, with a time delay of 5,000 y:

$$O(t) = O_1 \left( 1 - O_2 \frac{ds(t-5,000)}{dt} \right). \quad [3]$$

With the parameter values adopted ( $O_1 = 5.3 \text{ Tmol C yr}^{-1}$  and  $O_2 = 50 \text{ Tmol C m}^{-1}$ ), volcanic outgassing does not change by more than 30% during all glacial cycles. Note that over one glacial cycle, the average value of  $O$  is very close to

$O_1$ . The airborne flux of volcanic  $\text{CO}_2$  ("O") is one of the components of our Earth reservoir model (see expression 2). In *SI Appendix, Fig. S2B*, fluxes from two of the study experiments are depicted, comparing experiments with and without interactive ice sheets. The airborne flux of volcanic  $\text{CO}_2$  (O) is lower than the rest of fluxes involved in the calculation of the Earth reservoir.

In previous simulations with the climate model, certain carbon model state variables in Eq. 2 above, including airborne volcanic  $\text{CO}_2$  flux, atmospheric consumption of  $\text{CO}_2$  due to terrestrial weathering of carbonate and the silicate flux, were specified with 32-bit single precision values. In the current version, these parameters are instead specified in 64-bit double precision. As discussed in the main article, this seemingly minor change has profound impacts on the model simulations since small differences become significant for very long-term integrations.

**Experimental Design.** CLIMBER-2 experiments were performed from  $-3$  My to Present, in a single run, driven by only three forcings: solar insolation forcing (48), a gradual decrease in volcanic outgassing (30), and gradual regolith removal due to basal ice interactions (19). The configuration is similar to ref. 19, but our current study has not used the time-splitting technique.

*SI Appendix, Fig. S1* details the forcings prescribed in the experiments presented in this study: standard forward-in-time experiment (FIT) that reproduces the proxies (Fig. 1A), experiments gradually removing mechanisms by keeping them at a constant value (Fig. 1, panels BCDE) and back-in-time (BIT) experiment (Fig. 3, red). The BIT experiment was designed by reversing all forcings: solar cycle (eccentricity, obliquity, and longitude of perihelion), prescribed volcanic outgassing, and sediment masks. After the simulation was run, the time axis was flipped (21).

**Volcanic  $\text{CO}_2$  Outgassing Scenarios.** The present-day volcanic outgassing used in the model is  $5.3 \text{ Tmol C yr}^{-1}$ , which is the value that balances the average weathering rate. To derive the volcanic outgassing over time curve in the FIT experiment (*SI Appendix, Fig. S1A*), we followed the procedure in ref. 19 and constrained the value of  $\text{CO}_2$  volcanic outgassing using the best fit with observations. We then experimented with volcanic outgassing fixed at various levels between 5.2 and  $6.3 \text{ Tmol C yr}^{-1}$  (Fig. 2). This procedure implicitly subsumes other uncertainties, for example, the accuracy of the model representation of certain processes, in the estimation of volcanic outgassing.

**Regolith Cover Scenario.** For the FIT experiment, the regolith mask is similar to ref. 19 and is shown in *SI Appendix, Fig. S1A* (Bottom panel). We experimented with running simulations under a constant regolith cover mask, with regolith either undepleted (value set to extensive coverage of 3 My ago) or depleted (low coverage from Present). The depleted present-day regolith is characterized by exposed bedrock over large parts of northern North America and Eurasia, resulting from glacial erosion by Quaternary ice sheets.

Changes in regolith in the model impact the system via two mechanisms. Sliding velocity of ice is higher in the presence of thick regolith compared to exposed rocks (20), making ice sheets more mobile, thinner, and susceptible to orbital forcing. Moreover, greater regolith extent affects dust deposition over the ice sheets and thus albedo and surface mass balance.

**Ice-Sheet Model.** The ice sheet component of the model is described in ref. 30. The CLIMBER-2 incorporates the 3D thermomechanical ice sheet model SICOPOLIS (50) and a deep permafrost module (51, 52). The ice-sheet model is applied only to the Northern Hemisphere, with an assumed additional 10% contribution of the Antarctic ice sheet to sea level variations. The atmosphere and ice sheets are coupled bidirectionally using a physically based energy balance approach (53).

The model includes a fully interactive dust cycle as described by Bauer and Ganopolski (54, 55), with the updates from Willeit and Ganopolski (36). The emission of glaciogenic dust is taken to be proportional to the delivery of glacial sediments to the edge of an ice sheet. The model includes parameterization of aeolian dust deposition on snow albedo (35).

Important feedbacks accounted for in the ice sheet module are the ice-surface elevation mass-balance feedback (56), the ice-albedo feedback (49), and the snow-albedo feedback (53). These mechanisms are important to amplify the transition from interglacial to glacial climate.

**Orbital Forcings.** Orbital forcings for the past 3 My are based on astronomical solutions (48). One of the experiments (Fig. 1E) was performed with constant insolation (*SI Appendix, Fig. S1E*).

Atmospheric  $\text{pCO}_2$  was initialized at the preindustrial level, 270 ppm, in all experiments except for the FIT simulation (Fig. 1A and *SI Appendix, Fig. S1A*), whose Initial conditions correspond to the Late Pliocene and were set at 360 ppm to reduce the time to reach equilibrium based on the prescribed volcanic outgassing.

**Data, Materials, and Software Availability.** All study data are included in the article and/or *SI Appendix*.

**ACKNOWLEDGMENTS.** This study was supported (J.C., M.E.M., I.M., and S.A.C.) by funding from the School of Arts and Sciences of the University of Pennsylvania. M.W. is funded by the German climate modeling project PalMod supported by the German Federal Ministry of Education and Research (BMBF) as a Research for Sustainability initiative (FONA) (Grant nos. 01LP1920B, 01LP1917D, and 01LP2305B). We thank both Mikhail Verbitsky and Hugues Goose for their helpful comments and constructive reviews.

Author affiliations: <sup>a</sup>Department of Earth and Environmental Science, University of Pennsylvania, Pennsylvania, PA 19104; <sup>b</sup>Department of Applied Physics, University of La Laguna, La Laguna 38200, Spain; and <sup>c</sup>Potsdam Institute for Climate Impact Research, Potsdam 14412, Germany

1. M. Milanković, *Théorie mathématique des phénomènes thermiques produits par la radiation solaire* (Gauthier-Villars, 1920).
2. K. Milankovitch, Kanon der Erdbestrahlung und seine Anwendung auf das Eiszeitenproblem. *R. Ser. Acad. Sci. Spec. Publ.* **133**, 1–633 (1941).
3. A. Berger, Milankovitch theory and climate. *Rev. Geophys.* **26**, 624–657 (1988).
4. A. Abe-Ouchi *et al.*, Insolation-driven 100,000-year glacial cycles and hysteresis of ice-sheet volume. *Nature* **500**, 190–193 (2013).
5. A. Ganopolski, Toward generalized Milankovitch theory (GMT). *Clim. Past.* **20**, 151–185 (2024).
6. D. Paillard, The timing of Pleistocene glaciations from a simple multiple-state climate model. *Nature* **391**, 378–381 (1998).
7. S. Rutherford, S. D'Hondt, Early onset and tropical forcing of 100,000-year Pleistocene glacial cycles. *Nature* **408**, 72–75 (2000).
8. J. Imbrie *et al.*, On the structure and origin of major glaciation cycles. The 100,000-year cycle. *Paleoceanography* **8**, 699–735 (1993).
9. M. Y. Verbitsky, M. Crucifix, D. M. Volobuev, A theory of Pleistocene glacial rhythmicity. *Earth Syst. Dyn.* **9**, 1025–1043 (2018).
10. M. E. Raymo, L. E. Lisiecki, K. H. Nisancioglu, Plio-Pleistocene ice volume, Antarctic climate, and the global  $\delta^{18}\text{O}$  record. *Science* **313**, 492–495 (2006).
11. R. Bintanja, R. S. W. van de Wal, North American ice-sheet dynamics and the onset of 100,000-year glacial cycles. *Nature* **454**, 869–872 (2008).
12. M. E. Raymo, The timing of major climate terminations. *Paleoceanography* **12**, 577–585 (1997).
13. J. Imbrie *et al.*, On the structure and origin of major glaciation cycles: 1. Linear responses to Milankovitch forcing. Linear responses to Milankovitch forcing. *Paleoceanography* **7**, 701–738 (1992).
14. R. François *et al.*, Contribution of Southern Ocean surface-water stratification to low atmospheric  $\text{CO}_2$  concentrations during the last glacial period. *Nature* **389**, 929–935 (1997).
15. A. Berger, X. S. Li, M. F. Loutre, Modelling northern hemisphere ice volume over the last 3 Ma. *Quat. Sci. Rev.* **18**, 1–11 (1999).
16. N. J. Shackleton, The 100,000-year ice-age cycle identified and found to lag temperature, carbon dioxide, and orbital eccentricity. *Science* **289**, 1897–1902 (2000).
17. A. Ganopolski, R. Calov, The role of orbital forcing, carbon dioxide and regolith in 100 kyr glacial cycles. *Clim. Past.* **7**, 1415–1425 (2011).
18. J. F. McManus, R. Francois, J.-M. Gherardi, L. D. Keigwin, S. Brown-Leger, Collapse and rapid resumption of Atlantic meridional circulation linked to deglacial climate changes. *Nature* **428**, 834–837 (2004).
19. M. Willeit, A. Ganopolski, R. Calov, V. Brovkin, Mid-Pleistocene transition in glacial cycles explained by declining  $\text{CO}_2$  and regolith removal. *Sci. Adv.* **5**, eaav7337 (2019).
20. P. U. Clark, D. Paillard, Origin of the middle pleistocene transition by ice sheet erosion of regolith. *Paleoceanography* **13**, 1–9 (1998).
21. J. Carrillo *et al.*, Path-dependence of the Plio-Pleistocene glacial/interglacial cycles. *Proc. Natl. Acad. Sci.* **121**, e2322926121 (2024).
22. G. H. Denton *et al.*, The last glacial termination. *Science* **328**, 1652–1656 (2010).
23. N. Jiao *et al.*, Microbial production of recalcitrant dissolved organic matter: Long-term carbon storage in the global ocean. *Nat. Rev. Microbiol.* **8**, 593–599 (2010).
24. J. D. Shackleton, M. J. Follows, P. J. Thomas, A. W. Omta, The mid-pleistocene transition: A delayed response to an increasing positive feedback? *Clim. Dyn.* **60**, 4083–4098 (2023).
25. T. Gerlach, Volcanic versus anthropogenic carbon dioxide. *Eos Trans. Am. Geophys. Union.* **92**, 201–202 (2011).
26. V. Brovkin *et al.*, Carbon cycle, vegetation, and climate dynamics in the Holocene: Experiments with the CLIMBER-2 model. *Glob. Biogeochem. Cycles* **16**, 86–1–86–20 (2002).
27. A. Ganopolski *et al.*, CLIMBER-2: A climate system model of intermediate complexity. Part II: Model sensitivity. Part II: model sensitivity. *Clim. Dyn.* **17**, 735–751 (2001).

28. O. Cartapanis, D. Bianchi, S. L. Jaccard, E. D. Galbraith, Global pulses of organic carbon burial in deep-sea sediments during glacial maxima. *Nat. Commun.* **7**, 10796 (2016).
29. T. J. Crowley, W. T. Hyde, Transient nature of late Pleistocene climate variability. *Nature* **456**, 226–230 (2008).
30. A. Ganopolski, V. Brovkin, Simulation of climate, ice sheets and CO<sub>2</sub> evolution during the last four glacial cycles with an Earth system model of intermediate complexity. *Clim. Past* **13**, 1695–1716 (2017).
31. P. U. Clark *et al.*, The Middle Pleistocene transition: Characteristics, mechanisms, and implications for long-term changes in atmospheric pCO<sub>2</sub>. *Quat. Sci. Rev.* **25**, 3150–3184 (2006).
32. G. A. Goss, A. D. Rooney, Variations in mid-Pleistocene glacial cycles: New insights from osmium isotopes. *Quat. Sci. Rev.* **321**, 108357 (2023).
33. N. G. Pisias, T. C. Moore, The evolution of Pleistocene climate: A time series approach. *Earth Planet. Sci. Lett.* **52**, 450–458 (1981).
34. G. Krinner, O. Boucher, Y. Balkanski, Ice-free glacial northern Asia due to dust deposition on snow. *Clim. Dyn.* **27**, 613–625 (2006).
35. A. Ganopolski, R. Calov, M. Claussen, Simulation of the last glacial cycle with a coupled climate ice-sheet model of intermediate complexity. *Clim. Past* **6**, 229–244 (2010).
36. M. Willeit, A. Ganopolski, The importance of snow albedo for ice sheet evolution over the last glacial cycle. *Clim. Past* **14**, 697–707 (2018).
37. L. E. Lisiecki, M. E. Raymo, A Pliocene–Pleistocene stack of 57 globally distributed benthic  $\delta^{18}O$  records. *Paleoceanography* **20**, 1003 (2005).
38. R. M. Spratt, L. E. Lisiecki, A late Pleistocene sea level stack. *Clim. Past* **12**, 1079–1092 (2016).
39. B. Bereiter *et al.*, Revision of the EPICA Dome C CO<sub>2</sub> record from 800 to 600 ky before present. *Geophys. Res. Lett.* **42**, 542–549 (2015).
40. C. W. Snyder, Evolution of global temperature over the past two million years. *Nature* **538**, 226–228 (2016).
41. D. Khider *et al.*, Pyleoclim: Paleoclimate timeseries analysis and visualization with Python. *Paleoceanography* **37**, e2022PA004509 (2022).
42. V. Brovkin *et al.*, Comparative carbon cycle dynamics of the present and last interglacial. *Quat. Sci. Rev.* **137**, 15–32 (2016).
43. K. L. Denman *et al.*, “Couplings between changes in the climate system and biogeochemistry” in *Climate Change 2007: The Physical Science Basis. Contribution of Working Group I to the Fourth Assessment Report of the Intergovernmental Panel on Climate Change The Physical Science Basis*, S. D. Solomon *et al.*, Eds. (Cambridge University Press, Cambridge, UK, 2007), pp. 499–587.
44. R. A. Berner, The long-term carbon cycle, fossil fuels and atmospheric composition. *Nature* **426**, 323–326 (2003).
45. P. Huybers, C. Langmuir, Feedback between deglaciation, volcanism, and atmospheric CO<sub>2</sub>. *Earth Planet. Sci. Lett.* **286**, 479–491 (2009).
46. B. Saltzman, *Dynamical Paleoclimatology: Generalized Theory of Global Climate Change* (Academic Press, 2002).
47. V. Brovkin, A. Ganopolski, D. Archer, G. Munhoven, Glacial CO<sub>2</sub> cycle as a succession of key physical and biogeochemical processes. *Clim. Past* **8**, 251–264 (2012).
48. J. Laskar *et al.*, A long-term numerical solution for the insolation quantities of the Earth. *Astron. Astrophys.* **428**, 261–285 (2004).
49. G. R. North, Analytical Solution to a Simple Climate Model with Diffusive Heat Transport. *J. Atmos. Sci.* **32**, 1301–1307 (1975).
50. R. Greve, Application of a polythermal three-dimensional ice sheet model to the greenland ice sheet: Response to steady-state and transient climate scenarios. *J. Clim.* **10**, 901–918 (1997).
51. K. A. Crichton, D. M. Roche, G. Krinner, J. Chappellaz, A simplified permafrost-carbon model for long-term climate studies with the CLIMBER-2 coupled earth system model. *Geosci. Model Dev.* **7**, 3111–3134 (2014).
52. M. Willeit, A. Ganopolski, Coupled Northern Hemisphere permafrost-ice-sheet evolution over the last glacial cycle. *Clim. Past* **11**, 1165–1180 (2015).
53. R. Calov, A. Ganopolski, M. Claussen, V. Petoukhov, R. Greve, Transient simulation of the last glacial inception. Part I: Glacial inception as a bifurcation in the climate system. *Clim. Dyn.* **24**, 545–561 (2005).
54. E. Bauer, A. Ganopolski, Aeolian dust modeling over the past four glacial cycles with CLIMBER-2. *Glob. Planet. Change.* **74**, 49–60 (2010).
55. E. Bauer, A. Ganopolski, Sensitivity simulations with direct radiative forcing by aeolian dust during glacial cycles. *Clim. Past* **10**, 1333–1348 (2014).
56. J. Weertman, Milankovitch solar radiation variations and ice age ice sheet sizes. *Nature* **261**, 17–20 (1976).